Staudigel, P.T., et al., 2022, Apparent preservation of primary foraminiferal Mg/Ca ratios and Mg-banding in recrystallized foraminifera: Geology, v. 50, https://doi.org/10.1130/G49984.1

Apparent preservation of primary foraminiferal Mg/Ca ratios and Mg-banding in recrystallized foraminifera

Philip Staudigel, Eleanor John, Ben Buse and Caroline Lear

Supplementary Methodology, Results and Discussion

EPMA preparation, data acquisition, and processing:

Tests of *M. aragonensis* were picked from the 300-425 µm fraction of each sample (ODP865 9H-6 0-4 cm and TDP20 20-25-3 65-75cm). All tests were cleaned by brief ultrasonication in deionized water and methanol prior to embedding in Bueler Epothin. Samples were left to harden at room temperature for at least 72 hours and polished using fine sandpapers and a 0.3um Al_2O_3 emulsion. Figures S-1 and S-2 show the polished surfaces, with areas highlighted where EPMA maps were taken.

The samples were coated with silver to minimize beam damage (Smith, 1986). A small number of samples and standards were coated at the same time in a Quorum Q150RS sputter coater (Quorum Technologies, Laughton, UK). Any differences in sample height and distance to the target were minimized to ensure the same coat thickness on the standard and the unknown (Jurek et al., 1994; Matthews et al., 2019).

Analysis was undertaken using a JEOL 8530F EPMA, at 15kV. Spectrometers, standards and background offsets are given in Table S-1. Mg was measured on two spectrometers to increase analytical sensitivity. Mn and Ag were measured on analytical points but not mapped; the later was measured to check coat thickness. The standards were calibrated at 10nA, with 10 seconds on peak and 5 seconds on each background position. Mg and Sr were measured in differential mode to suppress the 3rd order Ca Kα and 2nd order Ca Kα respectively, which occur adjacent to the peaks being measured.

Figure S1: “Glassy” Foraminifer from Middle Eocene sediments of the Kilwa Group, Tanzania, TDP. Red box highlights area where EPMA map (Figure 1, main text) was made.

Figure S2: “Early Eocene frosty” Foraminifer from ODP Site 865. Red box highlights area where EPMA map (Figure 1, main text) was made.

Element	Spectrometer	Standard	+Bkg (mm)	-Bkg (mm)
Mg	Sp 1, TAP and Sp 3, TAPH	MgO	6.2	4
Sr	Sp 2 TAP	SrSO4	4.2	4.2
Ca	Sp 4 PETH	Wollastonite	1.65	2.66
Ag	Sp 4 PETH	Ag-metal	3	3
Fe	Sp 5 LIFL	Fayalite	3.5	3.27
Mn	Sp 5 LIFL	Mn-metal	3.28	2.88

Table S-1: Element, standard and background offsets

Analytical points were made from which the background height was determined.
Measurements were made at 5nA using a 1µm beam and the count times are given in Table S-2

Element	Peak (sec)	+Bkg (sec)	-Bkg (sec)
Mg	60	30	30
Sr	60	30	30
Ca	10	5	5
Ag	40	20	20
Fe	30	15	15
Mn	30	15	15

Table S-2: Count times for analytical points

The samples were mapped at 80nA using a focused beam, and the pixel size was 0.9 µm with a 500 millisecond dwell time. The maps were exported as csv files and python scripts were created to subtract the background intensity as determined from the analytical points and to convert the files into a format for quantification in the Probe for EPMA software (Probe Software Inc, Eugene, US). The maps were quantified using the Armstrong phi-rho-z model (Armstrong, 1988).

The processed EPMA data were exported as a .tiff file of element ratios (Mg & Sr) relative to calcium, pixels with %Ca values less than 36% were masked from further processing, in order to omit non pure calcium carbonate pixels from analysis. These .tiff files were read into a Matlab script which generated the different maps shown in Figure 1 of the main text. Transects A-A' and B-B' are 4µm wide, and show a moving average (1000 points spanning the range of the transect), where all data in the transect were weighted according to their distance from the point in question point. The position of a given point along the transect is defined by its distance to the left side of the transect. The distance along transect is calculated by applying a rotation matrix to the X and Y coordinates such that the transect is horizontal and this rotated coordinate system gives the position along the transect and distance from the transect. The new coordinates (x(i) and y(i)) for a point are calculated by first shifting the X and Y coordinates (from the original EPMA image, relative to the bottom-left corner) such that the left most point of the transect (X_L,Y_L) is the new origin, then the coordinates X_i Y_i are multiplied by a rotation matrix, M_{rot}.

$$\begin{bmatrix} x_i \\ y_i \end{bmatrix} = M_{rot} \begin{bmatrix} X_i - X_L \\ Y_i - Y_L \end{bmatrix} \qquad \text{(Equation S-1)}$$

In this equation, M_{rot} is calculated as a standard two-dimensional rotation matrix, where θ is the angle of the transect.

$$M_{rot} = \begin{bmatrix} cos(\theta) & -sin\,(\theta) \\ sin\,(\theta) & cos\,(\theta) \end{bmatrix} \qquad \text{(Equation S-2)}$$

A mask is applied to omit any data where y is not within ±2µm of the centerline of the transect. The weighting function (in this case the weight is shown for datapoint i with relative to position x(j) along the transect) is defined by a gaussian normal distribution function (σ = 1/3 µm) of according to the following

$$Weight(i,j) = \frac{1}{\sigma\sqrt{2\pi}} e^{\frac{-1}{2}\left(\frac{x(i)-x(j)}{\sigma}\right)^2} \qquad \text{(Equation S-3)}$$

In the above function, x(i) is the x-coordinate (along the transect) for measured datapoint (or pixel in elemental map) i and x(j) is the x-coordinate of the mean function at position j. From this, the mean value (in this case for Mg/Ca) at position x(j) of the transect is given from the following.

(Equation S-4)

In the above and following equation, n refers to the total number of unmasked datapoints (i.e points shown on the transect). The uncertainty (here again written for Mg/Ca) is shown in figure 1 of the main text as shaded region defined by the mean value ±1 weighted standard deviation ($\sigma_j^{weighted}$), given by the following.

$$\sigma_j^{weighted} = \sum_{i=1}^{n} Weight(i,j) \qquad \text{(Equation S-5)}$$

The mean value function A–A' from the TDP foraminifer is used as the initial condition for all subsequently described models, it is resampled in these models by interpolation to the appropriate number of cells (N=100 for all 1-D models in this manuscript).

Multiple tests of *M. aragonensis* from ODP Site 865 were analyzed using ICP-MS in order to validate the absolute values for Mg/Ca and Sr/Ca. The mean and standard deviation for the Mg/CA EPMA map are 4.23 ± 1.76 mmol/mol which can be compared with the ICP-MS value of 4.71 ± 0.72 (2 std). EPMA estimates Sr/Ca as 1.24 ± 0.72 mmol/mol, and ICP-MS estimates it as 0.94 ± 0.39. The range of uncertainty for the EPMA Mg/Ca is representative of the internal heterogeneity of the sample (i.e. Mg-banding), accounting for the number of datapoints (for example, by calculating the standard error) reduces these uncertainties to 0.02–0.01 mmol/mol for Mg and Sr respectively, however this would not account for uncertainty due to instrumental biases. It is unclear if there is a systematic difference EPMA and ICP-MS Mg/Ca measurements is due to a sub-sampling issue or due to differences in instrumental calibration, however the EPMA results for Sr/Ca and Mg/Ca each fall within the range of uncertainty of the ICP-MS measurements.

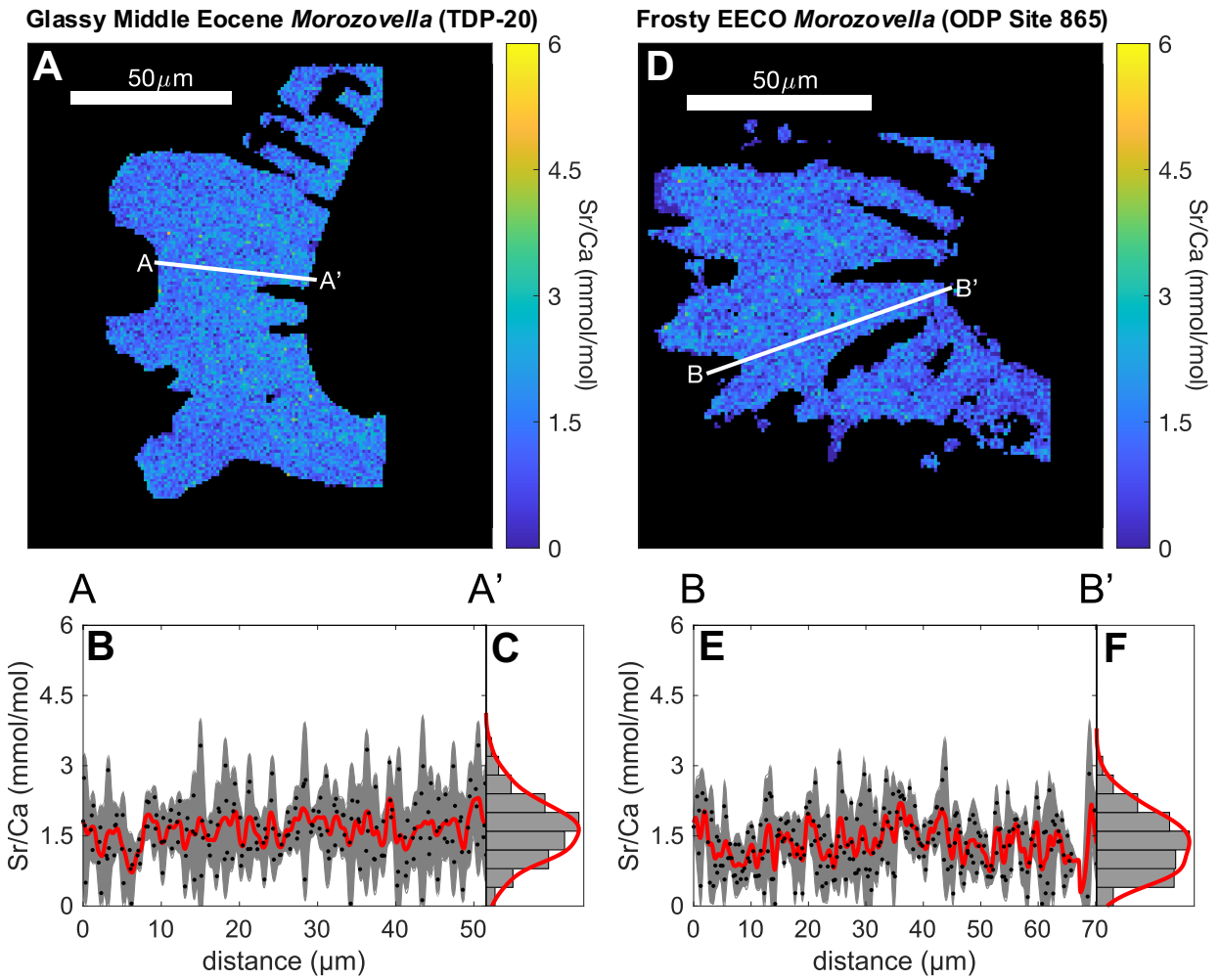

Figure S-3: Eocene *M. aragonensis*. A) EPMA Sr/Ca map of a glassy test from TDP Core 20. B) Transect A-A' Sr/Ca values. C) Histogram and Kernel density of Mg/Ca values across transect A-A' D) EPMA Sr/Ca map of a frosty test from ODP Site 865 E) Transect B-B' Mg/Ca values F) Histogram and Kernel density function of Mg/Ca values across transect B-B'.

Foraminiferal Stable Isotope and Trace Element Analyses:

Thirty to forty tests of *M. aragonensis* were picked from the 300-355μm fraction from the same depth (for Site 865) or biostratigraphic interval "Biozone E7/E8" (for TDP) as the EPMA samples. Tests were broken between glass plates, inspected under the microscope and impurities remaining in the inner chambers were removed with a wet brush. A split of these fragments was removed for stable isotope analysis, this split was cleaned in methanol and ultrasonicated prior to analysis. Stable isotope values ($\delta^{18}O$ and $\delta^{13}C$) were determined using a Thermo MAT 253 coupled to a Kiel IV carbonate preparation device at Cardiff University. Stable isotope results are reported relative to the Vienna Pee Dee Belemnite (VPDB) standard, with an external analytical precision of ±0.024‰ for $\delta^{13}C$ and ±x0.036‰ for $\delta^{18}O$ based on 154 replicate analyses of an in-house Carrara Marble standard calibrated to NBS-19. Bulk Mg/Ca and Sr/Ca measurements were made on the other split using a ICP-MS. Samples were prepared

following the cleaning procedure outlined by Barker et al., (2003), dissolved and analyzed using a Thermo Scientific ELEMENT-XR HR-ICP-MS in the CELTIC lab at Cardiff University. All whole-test isotope and trac element results for are presented in Table S-3.

Whole-test foraminiferal composition:

Location	Species	Mg/Ca (mmol/mol)	Sr/Ca (mmol/mol)	$\delta^{13}C$	$\delta^{18}O$	notes
TDP20	*M. aragonensis*	4.49 ± 0.07[!]	1.46 ± 0.67[!]	+3.33‰	-3.52‰	300-355µm multiple specimens
865B 12-1 (050-054cm)	*M. aragonensis*	3.85 ± 0.62[!]	0.95 ± 0.66[!]			300-355µm multiple specimens
865B 9-6 (000-004cm)	*M. crater*	4.76 ± 0.39[!]	0.92 ± 0.72[!]	+2.35‰	-1.73‰	300-355µm multiple specimens
TDP20 20-25-365-75cm	*M. aragonensis*	4.978[#]	1.53[#]			Mean EPMA values.
Site 865 (000-004cm)	*M. aragonensis*	4.231[#]	1.25[#]			EPMA for Mg/Ca, Sr/Ca, multiple specimen of same species for $\delta^{13}C$,$\delta^{18}O$
Site 865 (000-004cm)	*M. aragonensis*	4.71 ± 0.72[!]	0.94 ± 0.39[!]	+2.65‰	-1.78‰	Same specimen as EPMA, but measured using ICP-MS

Table S-3) Trace element data from Early Eocene. Paired $\delta^{18}O$ and Mg/Ca value are shown as points in Figure 2 in the main text.

[!]) Mg/Ca and Sr/Ca determined using ICP-MS

[#]) Mg/Ca and Sr/Ca determined from EPMA values

Description of reaction/diffusion model:

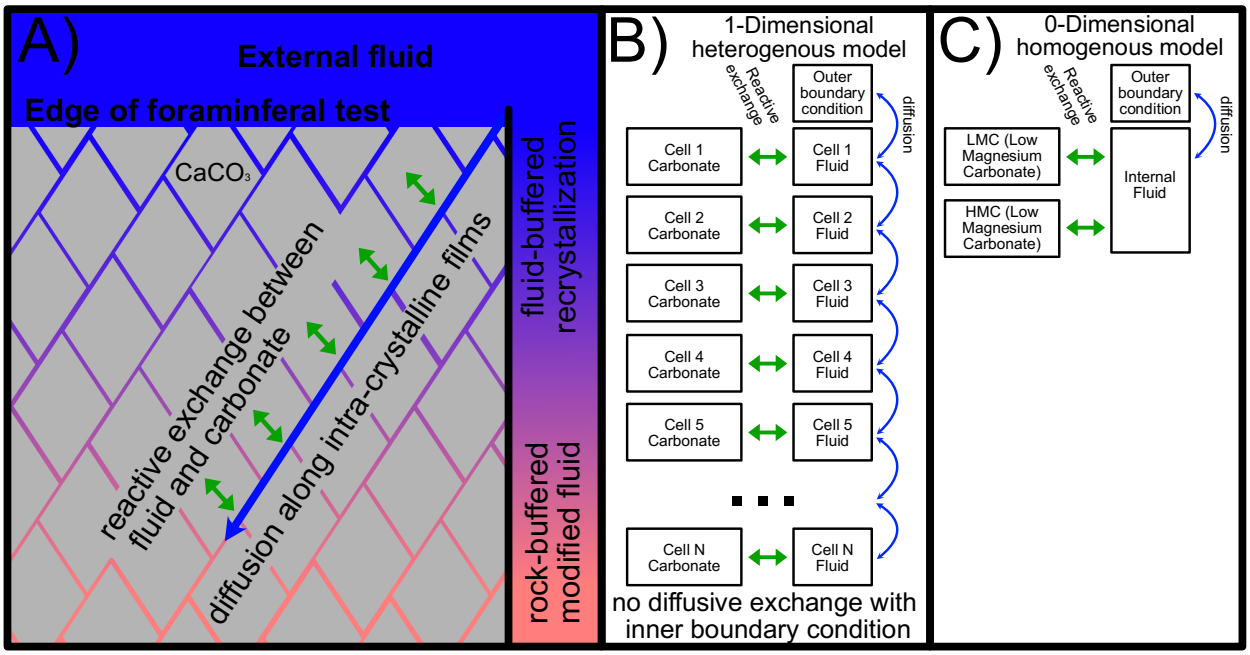

Figure S-4: Schematic diagram of conceptual and numerical models. A) Cartoon showing the modification of internal fluid via reactive exchange in a diffusively limited system. B) Diagram showing discretized implementation of "heterogenous" reactive-diffusive transport model C) Diagram showing implementation of "homogenous" reactive-diffusive model.

The model simulates the exchange of elements between a carbonate phase or phases and an internal water mass, which is able to diffusively exchange with outside water or adjacent water masses (Figure S-4). The alteration of heterogenous foraminiferal compositions is simulated using a 1-D reaction-diffusion model for the foraminiferal test (Figure S-4b). This approach is similar to that used by Ahm et al., (2018), although the model is functionally different, modeling carbonates as a single phase (as opposed to primary and diagenetic phases), simulating isotopes as separate species, and using a partitioning coefficient for Mg rather than a fixed Mg/Ca ratio in the diagenetic phase (this eliminates the possibility of negative Mg concentrations, which tend to stall the Ahm et al., model at faster exchange rates); a change which resulted in considerably greater stability and computational efficiency when running simulations with the different reaction rates necessary for this study. The simulation follows the conceptual model proposed by Wardlaw et al., (1978) where thin films of water facilitate the transition from a finer-grained primary material to a neomorphose secondary material. It is assumed that elements can diffuse along these water planes, which are connected to the exterior of the foraminiferal test. This is simulated using conventional water-carbonate system model, but with extremely low porosity. Metals (Ca^{2+}, Mg^{2+}, Sr^{2+}) as well as carbon and oxygen isotopes exchange with the carbonate phase, and form a diffusion gradient to the outer boundary condition. As reaction rates increase, the reactive term of this model exceeds the diffusive supply of ions, and thus the reaction is considered to be more "closed system" in nature. Because different elements are more abundant than others, not all elements are considered to be rock-buffered at certain reaction rates. Additionally, this model allows for compositional heterogeneity to be modeled during the same

reaction and diffusive processes, thus allowing features like Mg-banding to be evaluated numerically as a proxy for the preservation of primary Mg/Ca and Sr/Ca values.

The 1-D system is discretized into 100 cells of water and carbonate, where the relative portion of volume in each cell occupied by water is expressed as porosity (ϕ). These cells exchange with their neighbors via diffusion in the liquid phase (Fig. S-4b), this diffusion is assumed to behave according to Fick's law wherein flux is proportional to the concentration gradient. Thus, the change in concentration of a given species, i, with respect to time is proportional to the curvature of the concentration gradient, adjusted with a diffusivity coefficient, K_d. The rate of reaction, R, is defined as the fraction of carbonate equilibrated over a given time interval and is expressed in units of reciprocal time (s^{-1}).

The concentration of a given species, i, in the fluid ($C_{i,f}$), changes over time according to a one-dimensional reaction-diffusion equation given by the following

$$\frac{\partial C_{i,f}}{\partial t} = K_d \frac{\partial^2 C_{i,f}}{\partial z^2} + Rm\left(C_{i,s} - C_{i,eq}\right) \qquad \text{(Equation S-6)}$$

The concentration of the same species in the solid ($C_{i,s}$) is governed purely by the reactive term,

$$\frac{\partial C_{i,s}}{\partial t} = -R\left(C_{i,s} - C_{i,eq}\right) \qquad \text{(Equation S-7)}$$

The proportionality constant, m, is calculated according to the porosity of the unit (ρ_c), the density of the carbonate phase (ρ_c = 2.7g/cc) and the density of the fluid phase (ρ_w = 1.03 g/cc).

$$m = \frac{\rho_c(1-\phi)}{\rho_w \phi} \qquad \text{(Equation S-8)}$$

The equilibrium solid concentration ($C_{i,eq}$) of the species is calculated relative to the composition of the fluid phase and either a relative partitioning coefficient (D*) (Beattie et al., 1993) or a isotopic fractionation factor (α) for oxygen and carbon. The relative partitioning coefficient for a trace element (TE) in calcite is defined as

$$D^*_{TE} = \frac{C_{TE,eq}/C_{Ca,eq}}{C_{TE,f}/C_{Ca,f}} \qquad \text{(Equation S-9)}$$

The equilibrium concentration of magnesium is calculated with a relative partitioning coefficient of 0.012 (Mucci, 1987), and strontium is calculated with a value of 0.05 (Banner, 1995; Banner and Hanson, 1990). The equilibrium concentration of Ca, Mg and Sr in calcite are normalized such

that both charge balance (1 mol of calcite contains 1 mol of Ca+Sr+Mg), and the relative element ratios are respected as follows

$$C_{Ca,eq} = \frac{1}{1+D^*_{Mg}\frac{C_{Mg,f}}{C_{Ca,f}}+D^*_{Sr}\frac{C_{Sr,f}}{C_{Ca,f}}} \qquad \text{(Equation S-10)}$$

$$C_{Mg,eq} = \frac{D^*_{Mg}\frac{C_{Mg,f}}{C_{Ca,f}}}{1+D^*_{Mg}\frac{C_{Mg,f}}{C_{Ca,f}}+D^*_{Sr}\frac{C_{Sr,f}}{C_{Ca,f}}} \qquad \text{(Equation S-11)}$$

and

$$C_{Sr,eq} = \frac{D^*_{Sr}\frac{C_{Sr,f}}{C_{Ca,f}}}{1+D^*_{Mg}\frac{C_{Mg,f}}{C_{Ca,f}}+D^*_{Sr}\frac{C_{Sr,f}}{C_{Ca,f}}} \qquad \text{(Equation S-12)}$$

The isotope fractionation factor (α) is defined using a largely identical equation, except governed by the isotope ratios rather than elemental ratios.

$$\alpha_{calc-fluid} = \frac{R_{calcite}}{R_{fluid}} \qquad \text{(Equation S-13)}$$

The equilibrium fractionation of carbon is assumed to be temperature-insensitive in our model and is calculated as α = 1.001 (Romanek et al., 1992). The fractionation of oxygen is assumed to be driven by the temperature and is calculated as $1000\ln\alpha_{carb\text{-}water} = 18030 / T - 32.42$ (Kim and O'Neil, 1997). The ratio of isotopes is expressed using the conventional delta notation, following $\delta = (R_{sample}/R_{standard}\text{-}1) \times 1000‰$. R_{sample} is the ratio of isotopes of the element in question (e.g. $^{18}O/^{16}O$ or $^{13}C/^{12}C$) and $R_{standard}$ is the ratio of an isotopic standard, $R^{13}C_{PDB} = 0.01118$ (Chang and Li, 1990) and $R^{18}O_{PDB} = R^{18}O_{SMOW}*1.03092$ (Coplen et al., 1983) where $R^{18}O_{SMOW} = 0.0020052$ (Baertschi, 1976).

The diffusion coefficient (K) is calculated with respect to temperature for each species following the tables provided in chapter 4 of Boudreau, (1997). The self-diffusion of oxygen isotopes was calculated as a polynomial with respect to temperature following the results of (Simpson and Carr, 1958).

$$K_0^{oxygen} = (8.702 + 0.443T + 0.0035T^2)10^{-6}(c\,m^2/s) \qquad \text{(Equation S-14)}$$

The diffusivity is adjusted for tortuosity, where the tortuosity factor, θ^2, defined relative to porosity following the modified Maxwell-Weissburg relationship (Akanni et al., 1987; Boudreau, 1997; Maxwell, 1881; Petersen, 1958; Weissberg, 1963).

$$K = \frac{K_0}{\theta^2} \qquad \text{(Equation S-15)}$$

where

$$\theta^2 = 1 - ln(\phi^2) \qquad \text{(Equation S-16)}$$

A temperature of 12°C was used in these models, emulating bottom water temperatures in the early Eocene (Lear et al., 2000). Models were simulated using a reaction rate of 10^{-5}, 10^{-8} and 10^{-11} s^{-1}, which correspond roughly with recrystallization on the order of days, years and millennia, which will be referred to as the "closed" "semi-closed" and "open" models. It should be noted that, because the diffusivity and relatively unknown water-calcite ratios contribute significant uncertainty into the absolute rates of change in the model, these reaction rates could more realistically be described as simply changing the relative contribution of the reactive and diffusive fluxes in this system.

The relationship between the reactive and diffusive fluxes can be described using the lengthscale of a diffusive boundary layer (L_d) which, for a given species, is proportionate to the diffusive coefficient (K_d), the reaction rate (R), the mass-fluid molar ratio (M), and absolute partitioning coefficient (D) with the following relationship (Berner, 1980; Fantle et al., 2010).

$$L_d = \sqrt{\frac{\mathrm{D}}{RMK}} \qquad \text{(Equation S-17)}$$

The absolute partitioning coefficient (D) varies slightly from the prior definition for relative partitioning coefficient (D*), as it simply relates the concentration of an element in the fluid with the concentration of the element in the mineral phase, without normalizing it to another element, (e.g. calcium) (Henderson and Kracek, 1927). In the main text, this diffusive lengthscale is normalized to the model cell size to calculate the Normalized Diffusive Flux (NDF) parameter. Because many of these variables in Equation S-17 are directly affected by the porosity, the model assumes that the fluids account for 10^{-6} of the total volume of the foraminiferal test (representing a best-guess for the relative mass of intra-crystalline water films), this can be been treated as a variable in the presented model, however because the relative magnitude of diffusive supply and reactive modification is already governed by the reaction rate, the porosity was held constant in all models for the sake of consistency. Because of this, the model output should not be interpreted as resembling the absolute rate of alteration, but rather should be used as a means of exploring the relative rate of alteration for different element and isotope ratios within a foraminiferal test.

The outer boundary condition for these models are chosen to be representative of Eocene seawater, with a Mg/Ca molar ratio of 2.2 (Evans et al., 2018), a Sr/Ca molar ratio of 0.008 (Lear et al., 2003), an ice-free $\delta^{18}O$ value of -0.89‰ (Cramer et al., 2011). The benthic DIC $\delta^{13}C$ value of -0.8‰ was chosen to represent an equilibrium state with benthic foraminifera at ODP Site 865 reported by Sexton et al., (2006).

Simulations were run for the concentrations of Ca, Mg, Sr, ^{16}O, ^{18}O, ^{12}C and ^{13}C where the initial composition was derived from analyses of glassy TDP foraminifera. The initial state of the model

with respect to Mg/Ca and Sr/Ca heterogeneity (i.e. Mg-banding) was taken from transects across EPMA maps of the TDP foraminifera (Figure 1, main text). The initial $\delta^{18}O$ and $\delta^{13}C$ values were taken from the whole-test analyses of foraminifera from the same depth interval. In addition to these models, a second "homogenous" model is run, which is a simplified model with 1 box (Fig S-4c). The purpose of this model is to evaluate the system independently of the Mg-banding heterogeneity, so as to better compare the results to bulk measurements, which are more common in the literature, the initial state of this single box model is the mean values for the initial state of the heterogenous model. The zero-dimensional 1-box model models two solid phases, representing high-magnesium calcite and low-magnesium calcite, which account for 25% and 75% of the total carbonate, respectively. The composition of these two are identical, except in their Mg/Ca ratio, which is increased by 10mmol/mol in the HMC. The absolute values of these are calculated such that the bulk Mg/Ca is that of the initial sample. The HMC and LMC components can be modeled with different reactivities.

The model was implemented using Matlab™'s *ode15s* differential equation solver and is available to use and abuse by the reader as part of the supplementary documentation to this manuscript.

Parameter	Value or equation	Source
Oxygen isotope fractionation	$1000\ln(\alpha_{c-w}) = \frac{18030}{T} - 32.42$	(Kim and O'Neil, 1997)
Carbon isotope fractionation	$\alpha_{Carb-DIC} = 1.001$	(Romanek et al., 1992)
Partitioning Coefficient of Mg	$K_{Mg} = 0.012$; $K_{Mg} = 8.1 \times 10^{-4}$	(Mucci, 1987) ; (Baker et al., 1982)
Partitioning Coefficient of Sr	$K_{Sr} = 0.05$	(Banner, 1995)
Diffusion of Ca	$D^0_{Ca} = (3.60 + 0.144T[°C]) \times 10^{-6}$	(Boudreau, 1997)
Diffusion of Mg	$D^0_{Mg} = (3.43 + 0.144T[°C]) \times 10^{-6}$	(Boudreau, 1997)
Diffusion of Sr	$D^0_{Sr} = (3.69 + 0.169T[°C]) \times 10^{-6}$	(Boudreau, 1997)
Diffusion of DIC	$D^0_{Ca} = (5.06 + 0.275T[°C]) \times 10^{-6}$	(Boudreau, 1997)
Diffusion of O	$D^0_{Oxyen} = (8.702 + 0.443T[°C] + 0.0035T[°C]^2) \times 10^{-6}$	(Simpson and Carr, 1958).

Table S-4) Table of parameters used in model

Calculating paleotemperature:
Absolute paleotemperatures are calculated from whole-test $\delta^{18}O$ and Mg/Ca values.

The Mg/Ca value for *Morozovella* in the Eocene is calculated using the modern photosymbiont-bearing foraminifera species *T. sacculifer* (formerly *G. sacculifer;* Dekens et al., 2002).

$$\frac{Mg}{Ca_{foram}} = 0.37 \exp(0.090\ T) \qquad \text{(Equation S-18)}$$

The Mg/Ca of modern seawater is 5.2, this modern calibration is adapted to the Eocene Mg/Ca value of 2.2 following Evans et al., (2018).

$$Mg/Ca_{foram} = \left(\frac{0.37}{5.2^{H}}\right) * (Mg/Ca_{Eocene-SW})^{H} \exp(0.090\ T)$$ (Equation S-19)

Where H=0.41 derived from *G. sacculifer* by (Evans and Müller, 2012)

The equation used to calculate $\delta^{18}O$ temperatures for *Morozovella* is taken a modern *G. sacculifer*, (Mulitza et al., 2003).

$$\delta^{18}O_{\text{foram}} = \frac{T(^{\circ}C) - 14.91^{\circ}C}{-4.35} + \delta^{18}O_{\text{water}}$$ (Equation S-20)

In figures 2 and 3 of the main text, the $\delta^{18}O$ value for primary seawater is adjusted from the benthic $\delta^{18}O$ of -0.89‰ by +1.24‰, this is done such that Mg/Ca and $\delta^{18}O$-derived paleotemperatures are equivalent for the TDP *Morozovella*.

Supplementary Model Output figures:

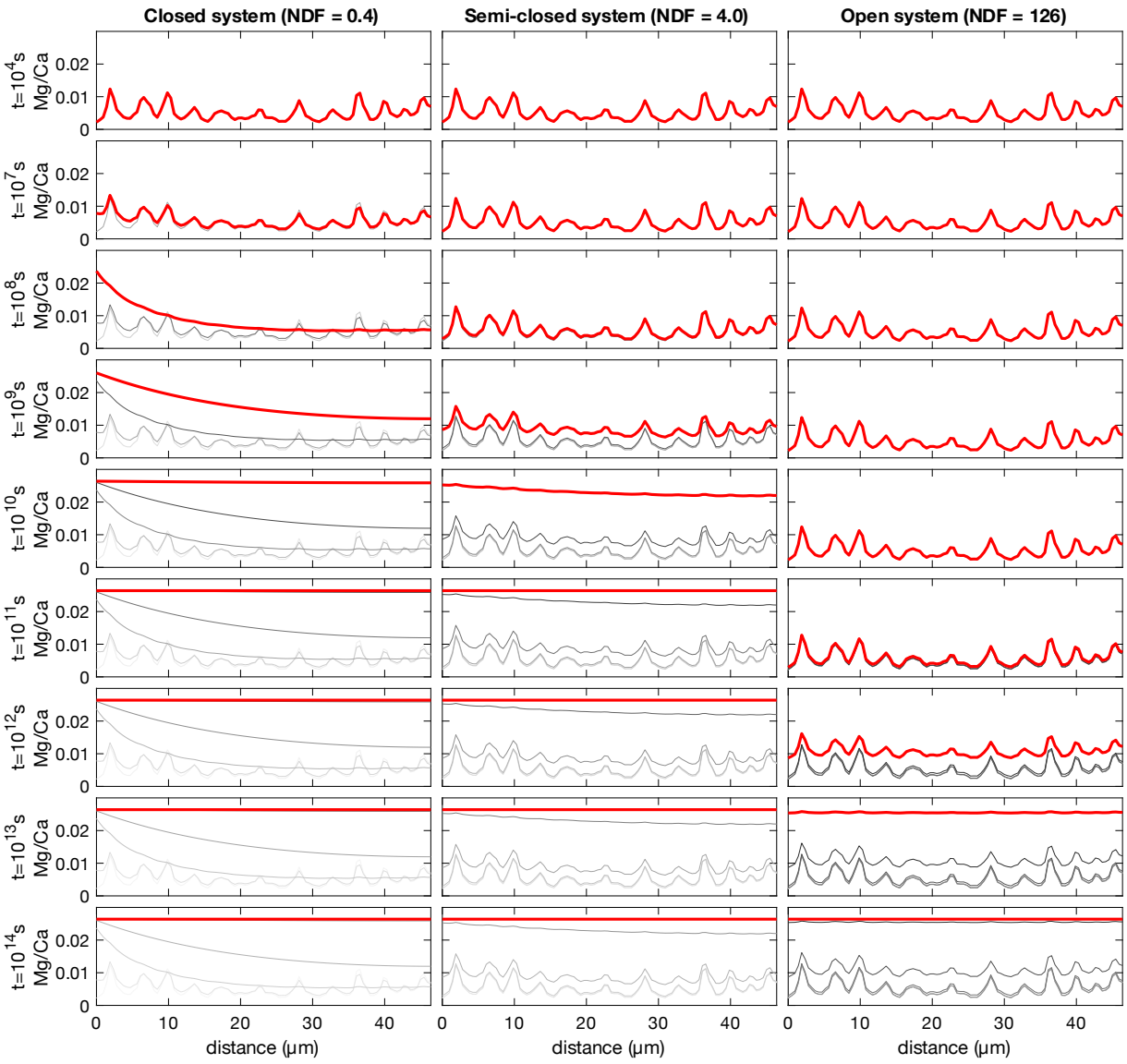

Figure S-5: Modeled Mg/Ca relative to distance along Transect A-A' from Figure 1 in main text, results for Closed, semi-closed and open models at selected timesteps, using distribution coefficient from Mucci, (1987). Bolded red line shows current timestep, gray lines show previous timesteps.

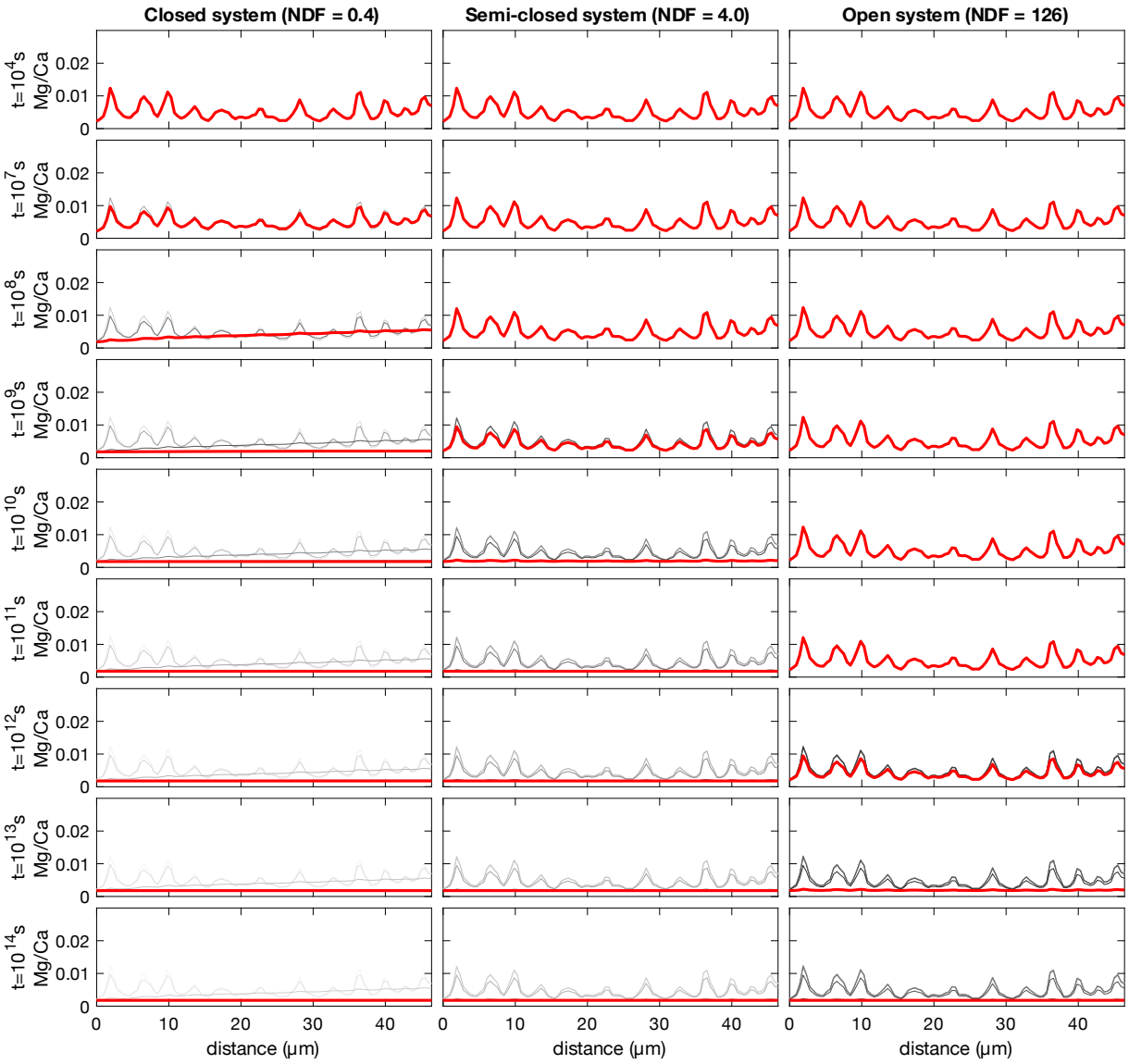

Figure S-6: Modeled Mg/Ca relative to distance along Transect A-A' from Figure 1 in main text, results for Closed, semi-closed and open models at selected timesteps, using distribution coefficient from Baker et al., (1982). Bolded red line shows current timestep, gray lines show previous timesteps.

All data from models discussed in the main text are shown here as supplementary figures showing the compositional values over time (left column), and as crossplots of all parameters (right columns).

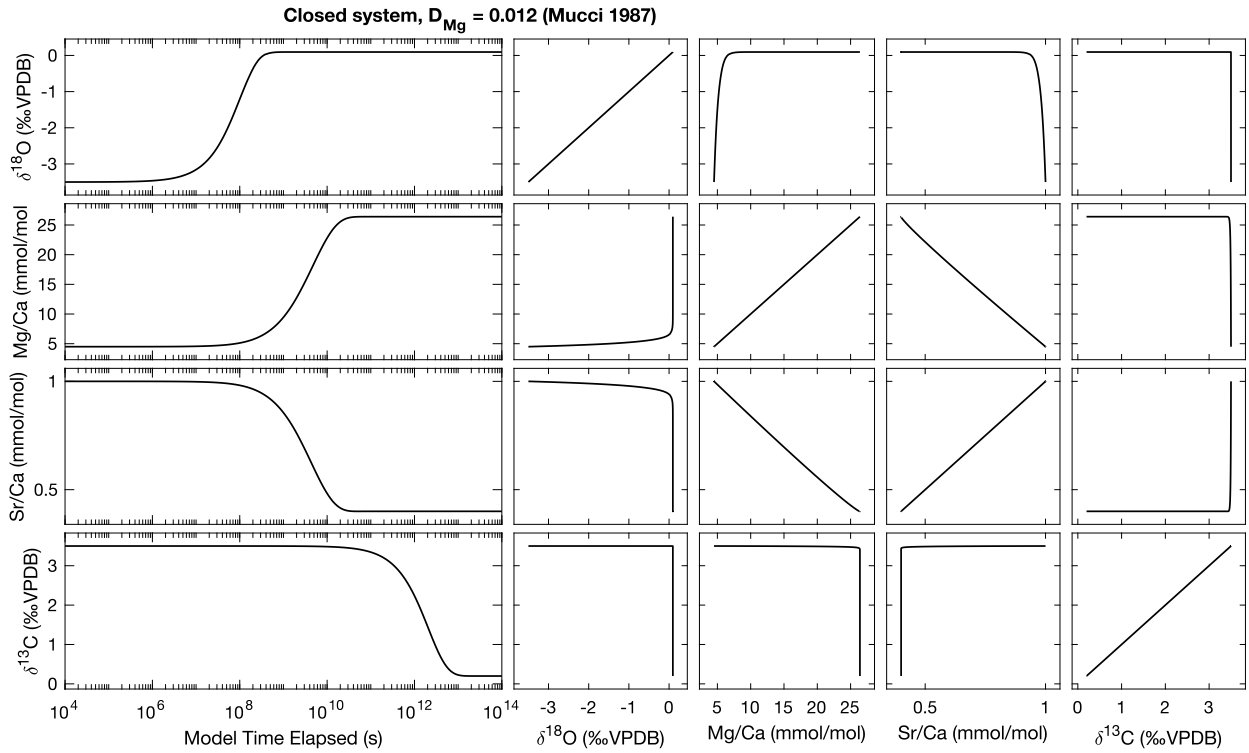

Figure S-7: “Closed system” model (NDF = 0.4) output for 0-D model using the Mucci (1987) Mg partitioning coefficient with equal reactivities for HMC and LMC.

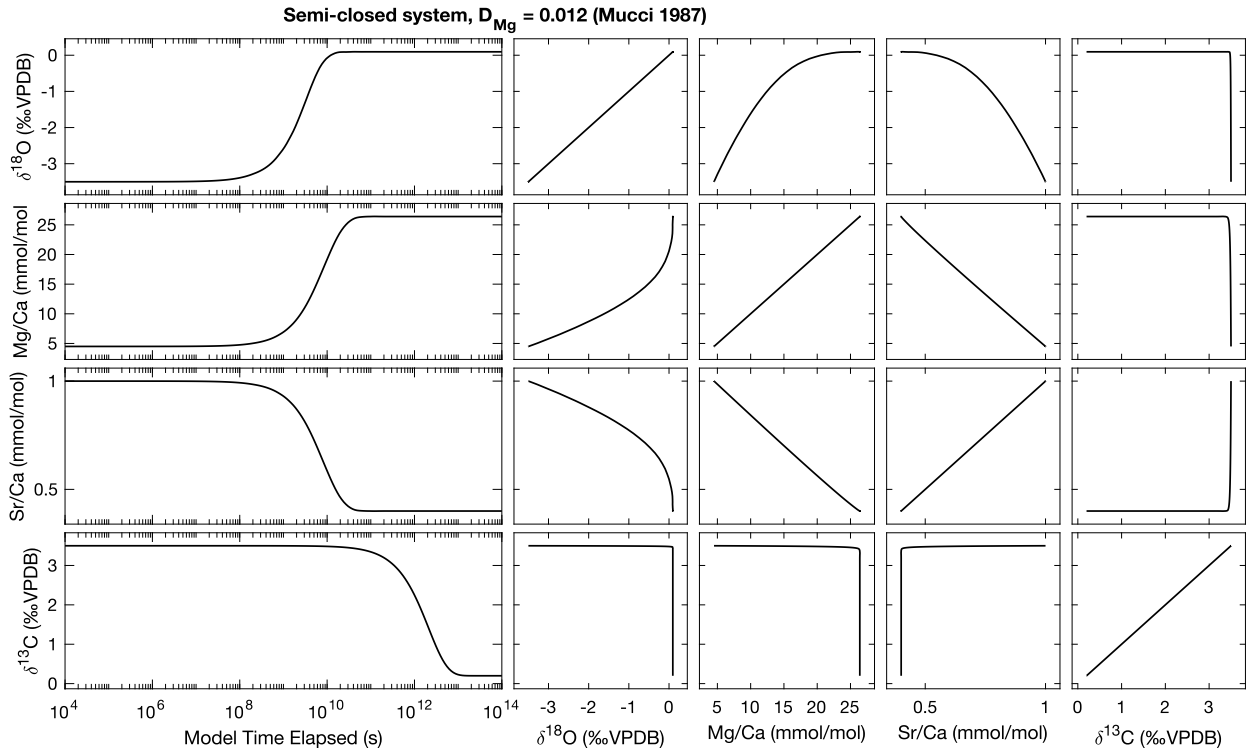

Figure S-8: "semi-closed system" model (NDF = 4.0) output for 0-D model using the Mucci (1987) Mg partitioning coefficient with equal reactivities for HMC and LMC.

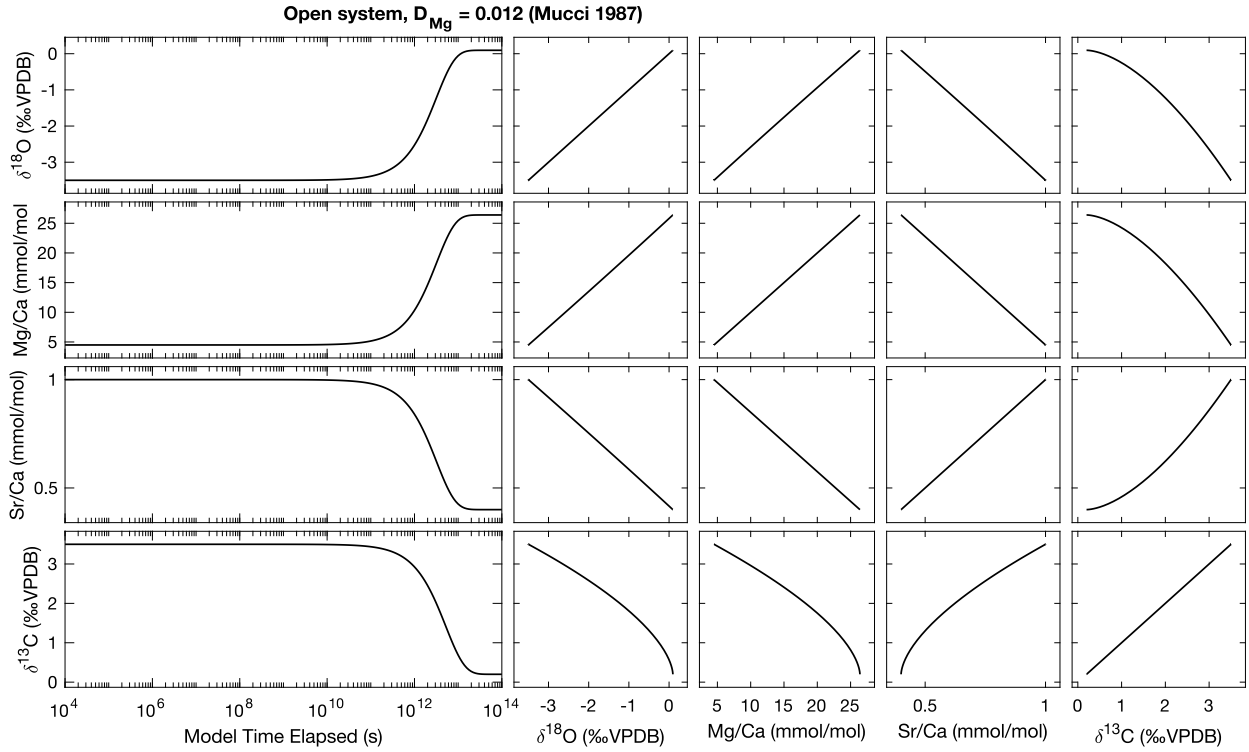

Figure S-9: "open system" model (NDF = 126) output for 0-D model using the Mucci (1987) Mg partitioning coefficient with equal reactivities for HMC and LMC.

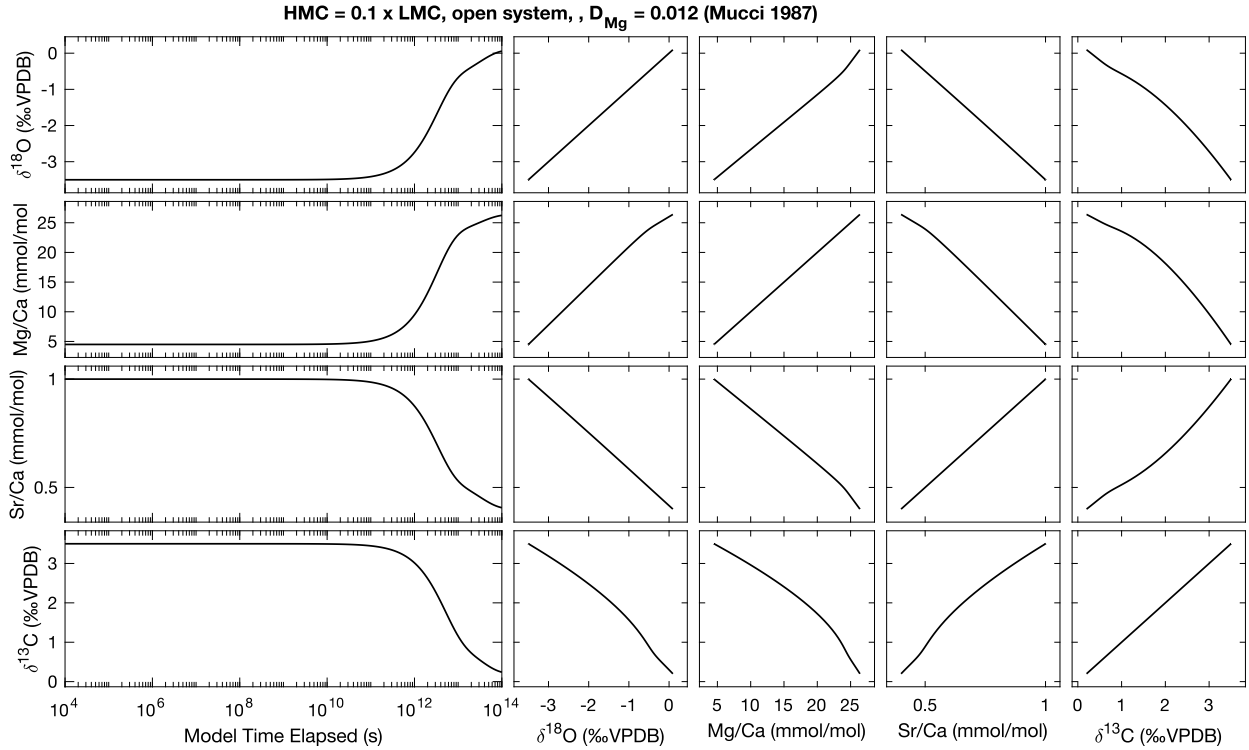

Figure S-10: “open system” model (NDF = 126) output for 0-D model using the Mucci (1987) Mg partitioning coefficient where the HMC component is 0.1x as reactive as LMC.

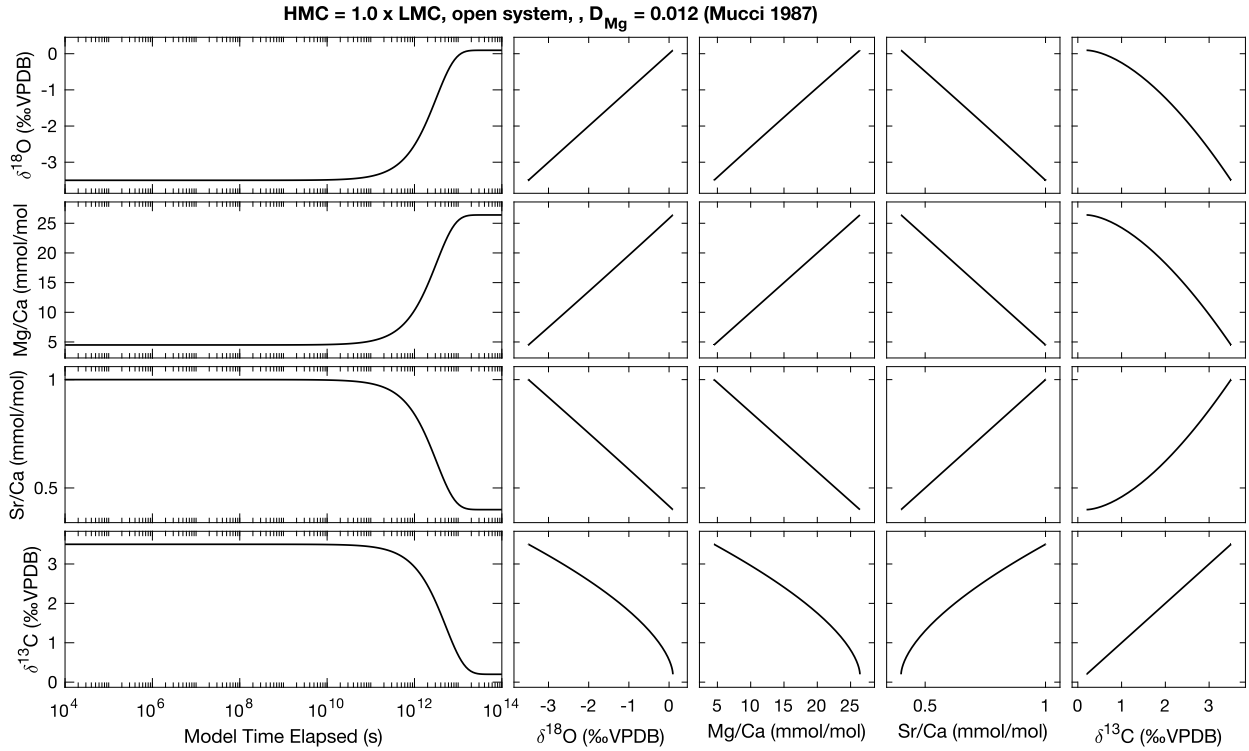

Figure S-11: “open system” model (NDF = 126) output for 0-D model using the Mucci (1987) Mg partitioning coefficient where the HMC component is as reactive as LMC.

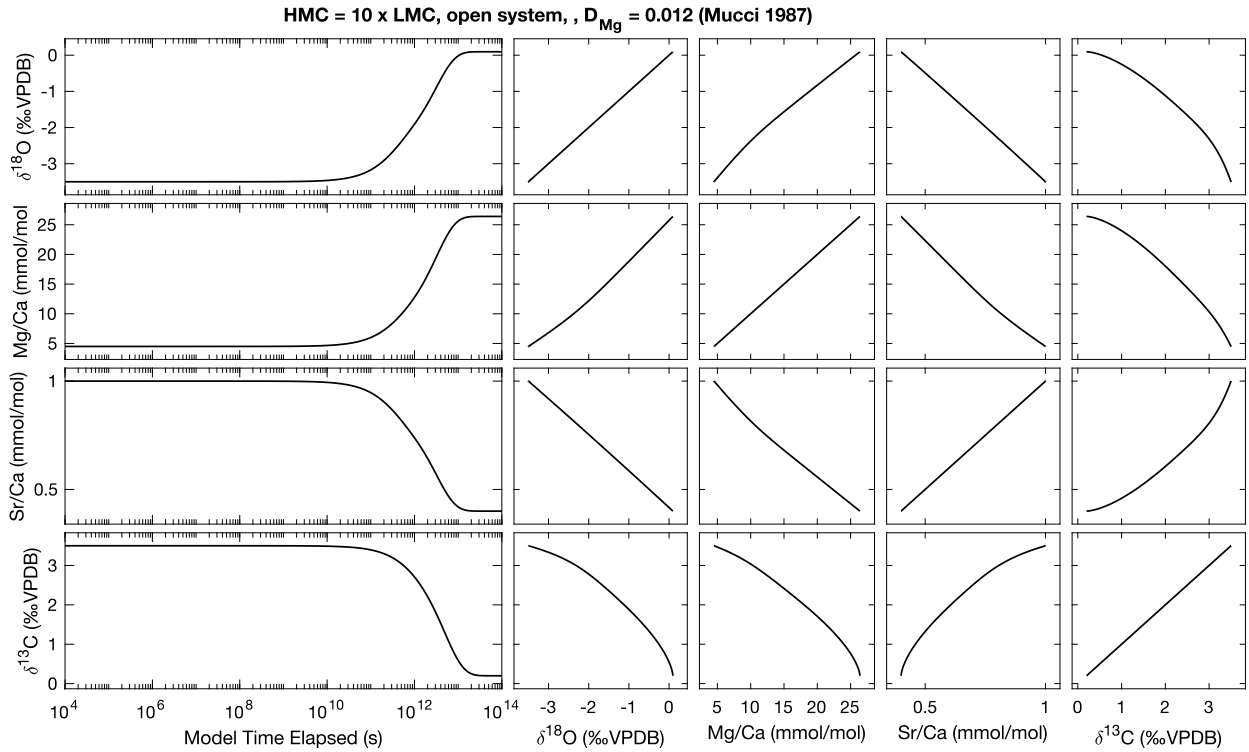

Figure S-12: "open system" model (NDF = 126) output for 0-D model using the Mucci (1987) Mg partitioning coefficient where the HMC component is 10x as reactive as LMC.

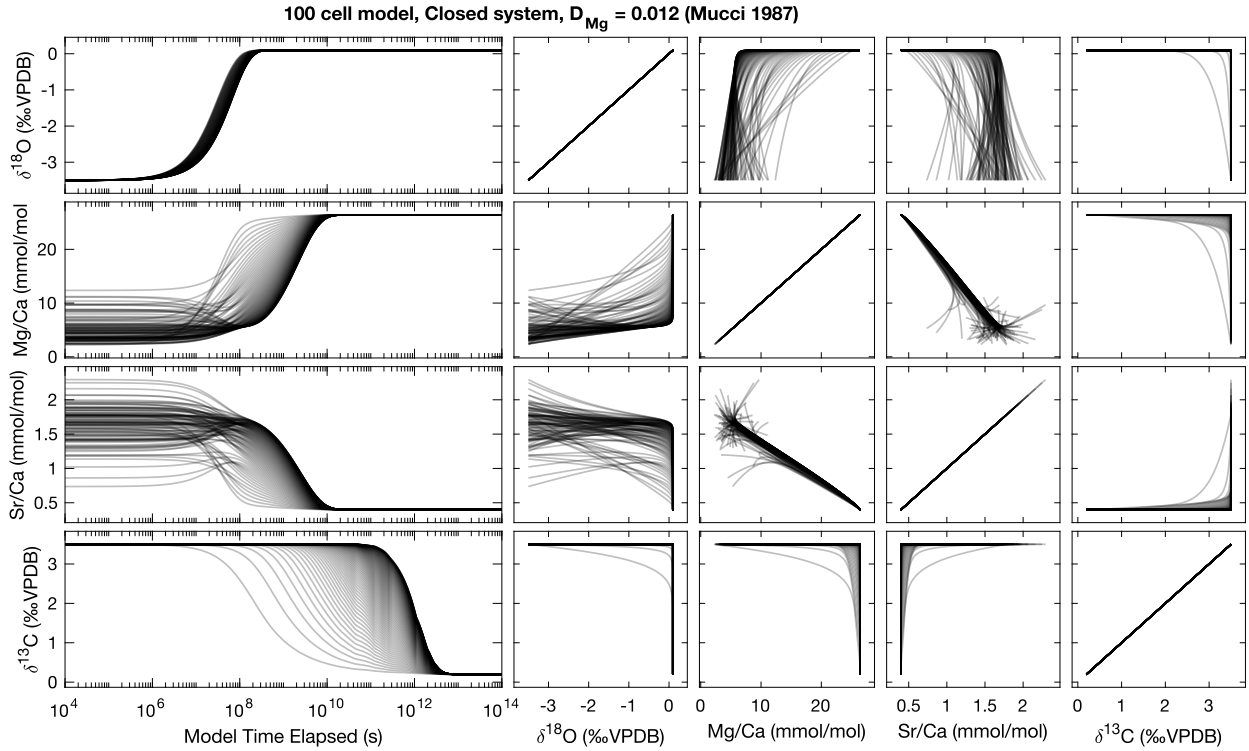

Figure S-13: "closed system" model (NDF = 0.4) output for 1-D model using the Mucci (1987) Mg partitioning coefficient with equal reactivities for HMC and LMC.

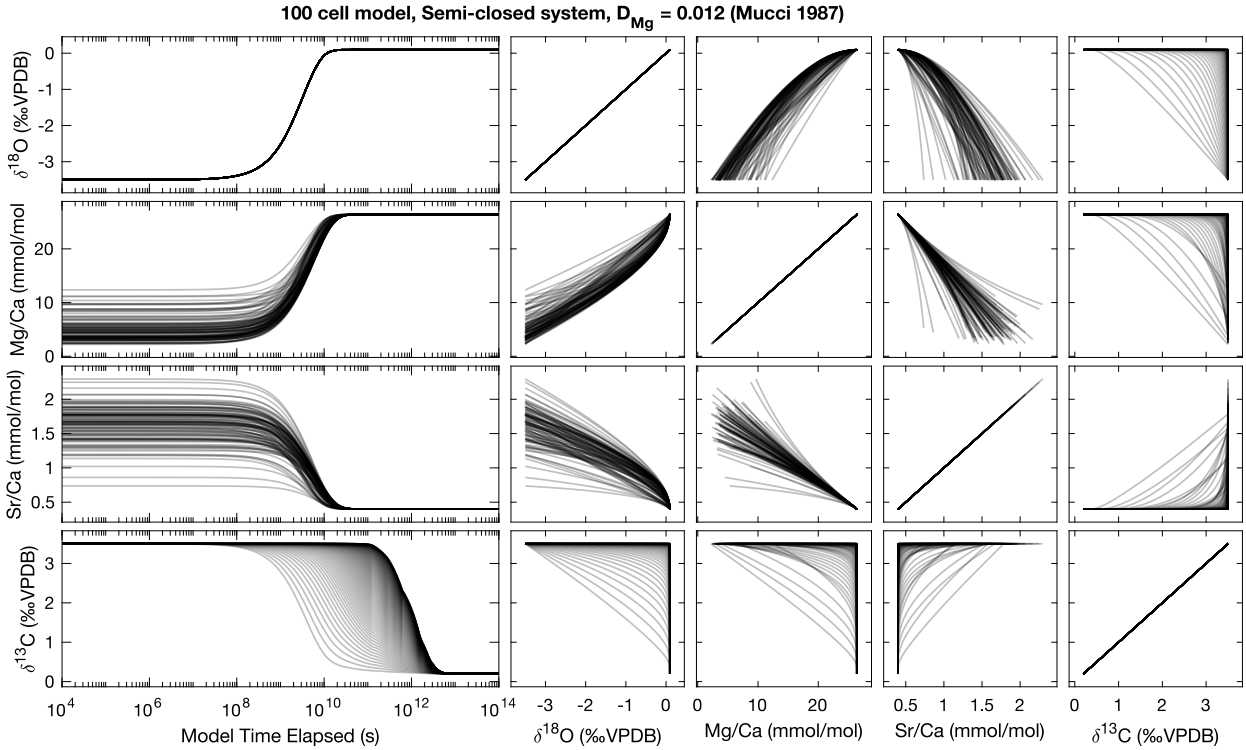

Figure S-14: "semi-closed system" model (NDF = 4) output for 1-D model using the Mucci (1987) Mg partitioning coefficient with equal reactivities for HMC and LMC.

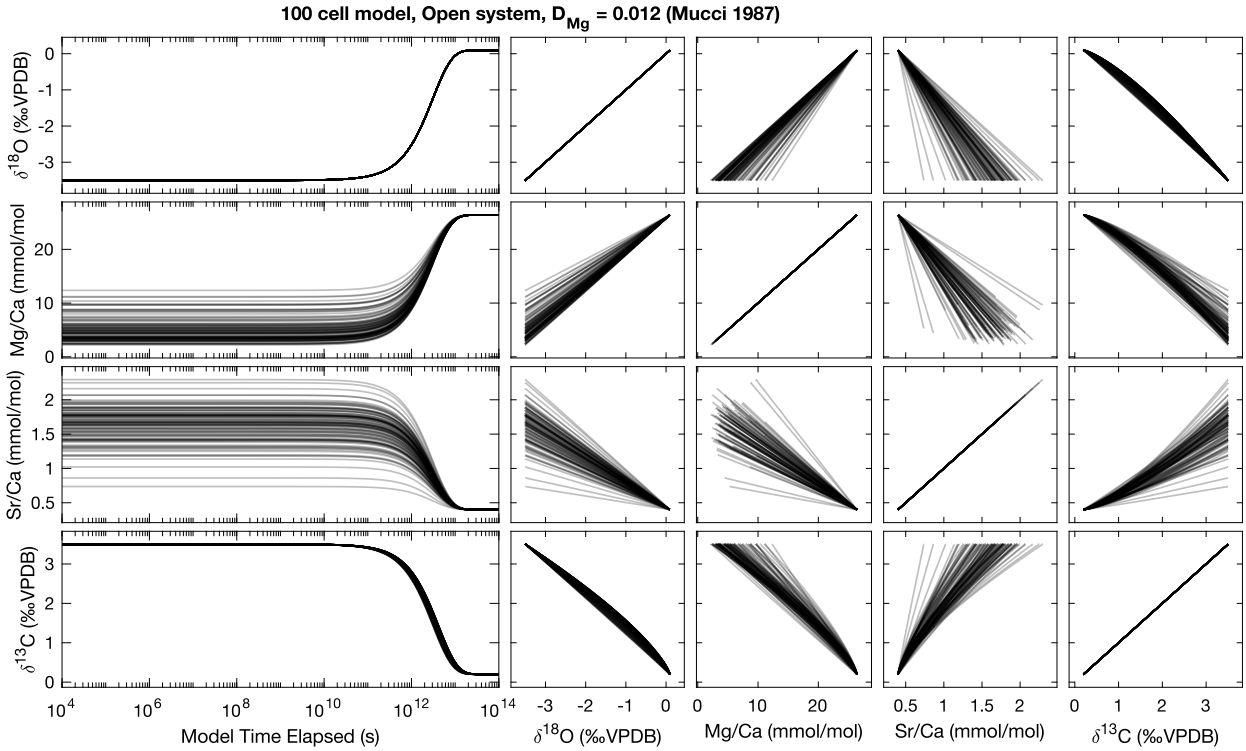

Figure S-15: "open system" model (NDF = 126) output for 1-D model using the Mucci (1987) Mg partitioning coefficient with equal reactivities for HMC and LMC.

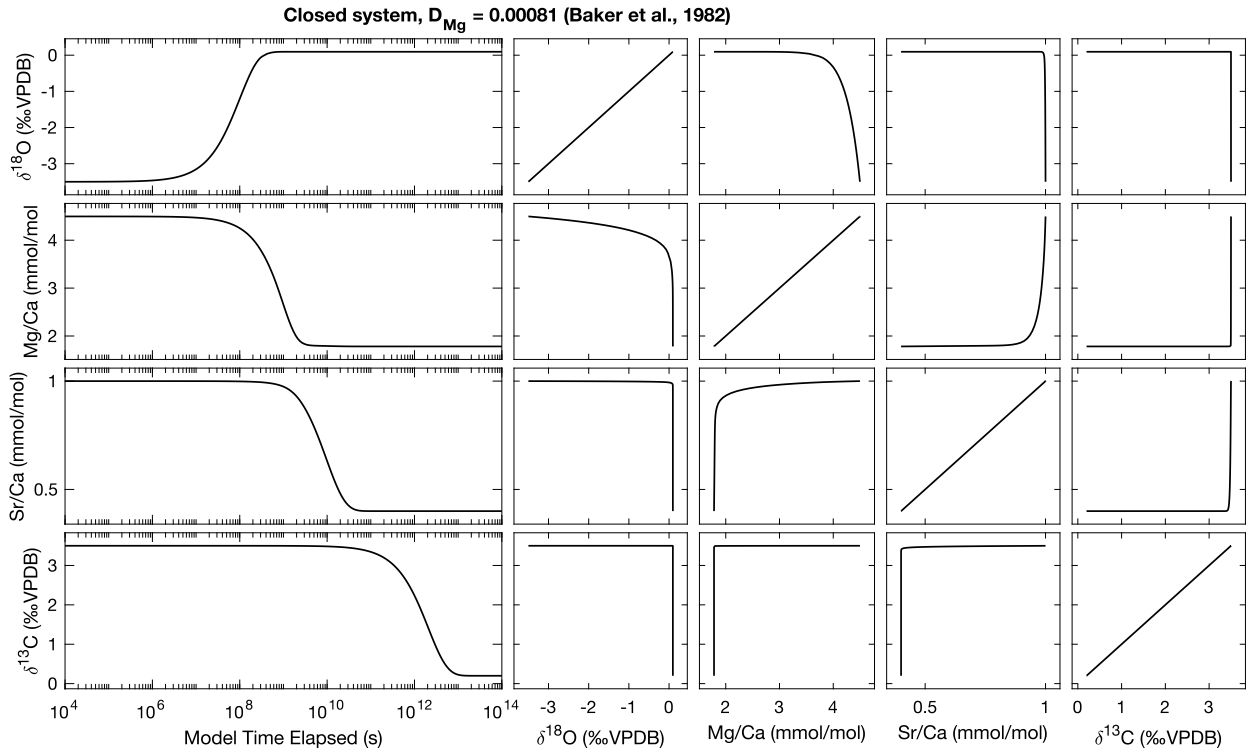

Figure S-16: “Closed system” model (NDF = 0.4) output for 0-D model using the Baker et al., (1982) Mg partitioning coefficient with equal reactivities for HMC and LMC.

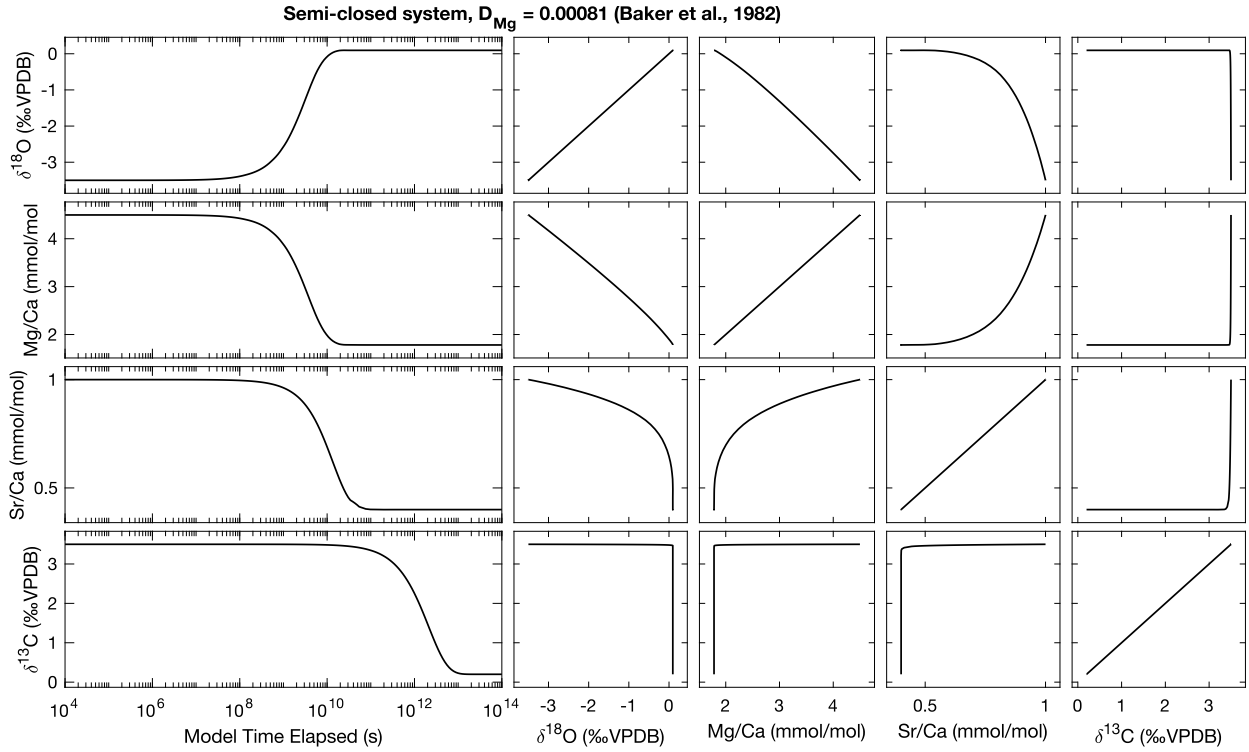

Figure S-17: “semi-closed system” model (NDF = 4.0) output for 0-D model using the Mucci (1987) Mg partitioning coefficient with equal reactivities for HMC and LMC.

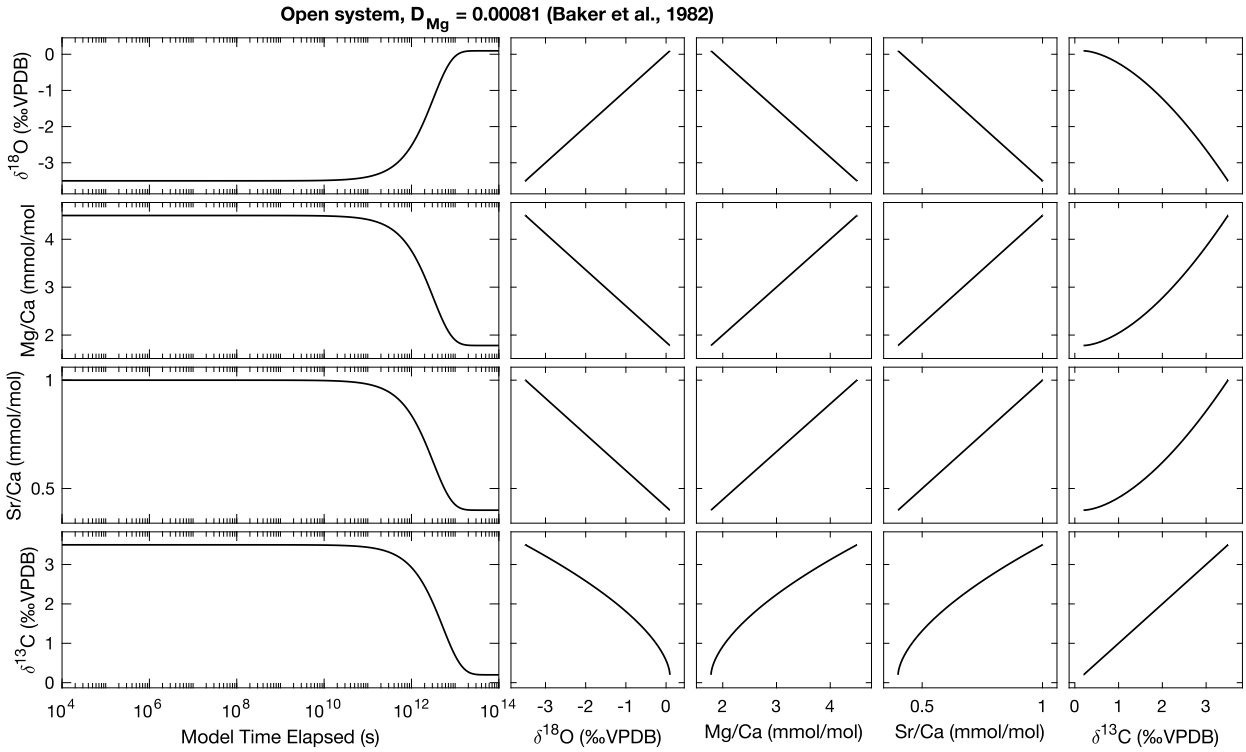

Figure S-18: “open system” model (NDF = 126) output for 0-D model using the Mucci (1987) Mg partitioning coefficient with equal reactivities for HMC and LMC.

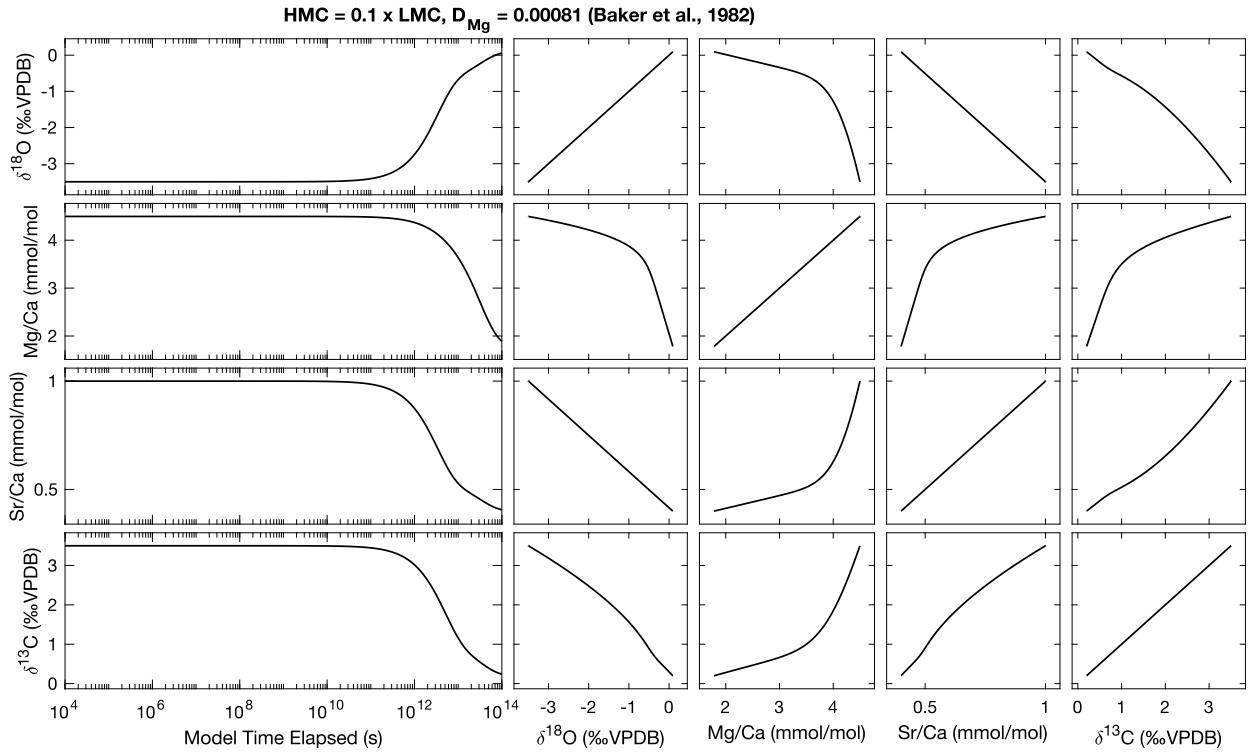

Figure S-19: "open system" model (NDF = 126) output for 0-D model using the Mucci (1987) Mg partitioning coefficient where the HMC component is 0.1x as reactive as LMC.

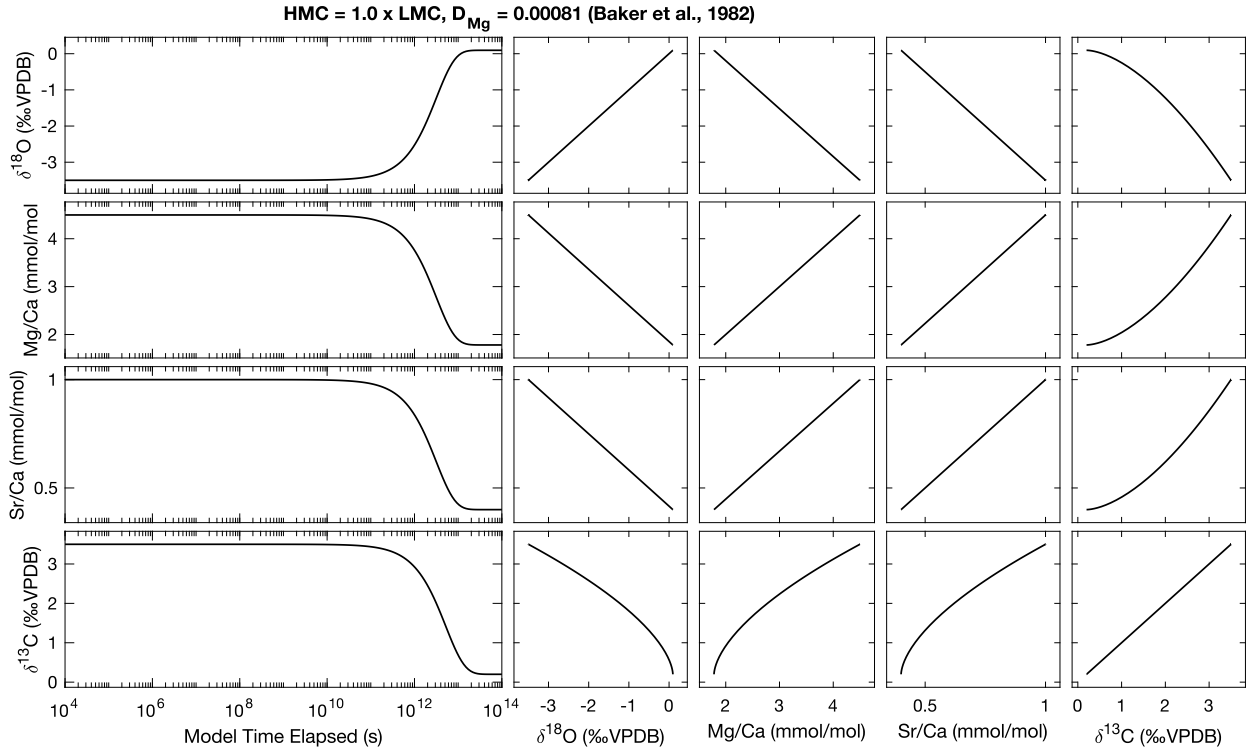

Figure S-20: "open system" model (NDF = 126) output for 0-D model using the Mucci (1987) Mg partitioning coefficient where the HMC component is as reactive as LMC .

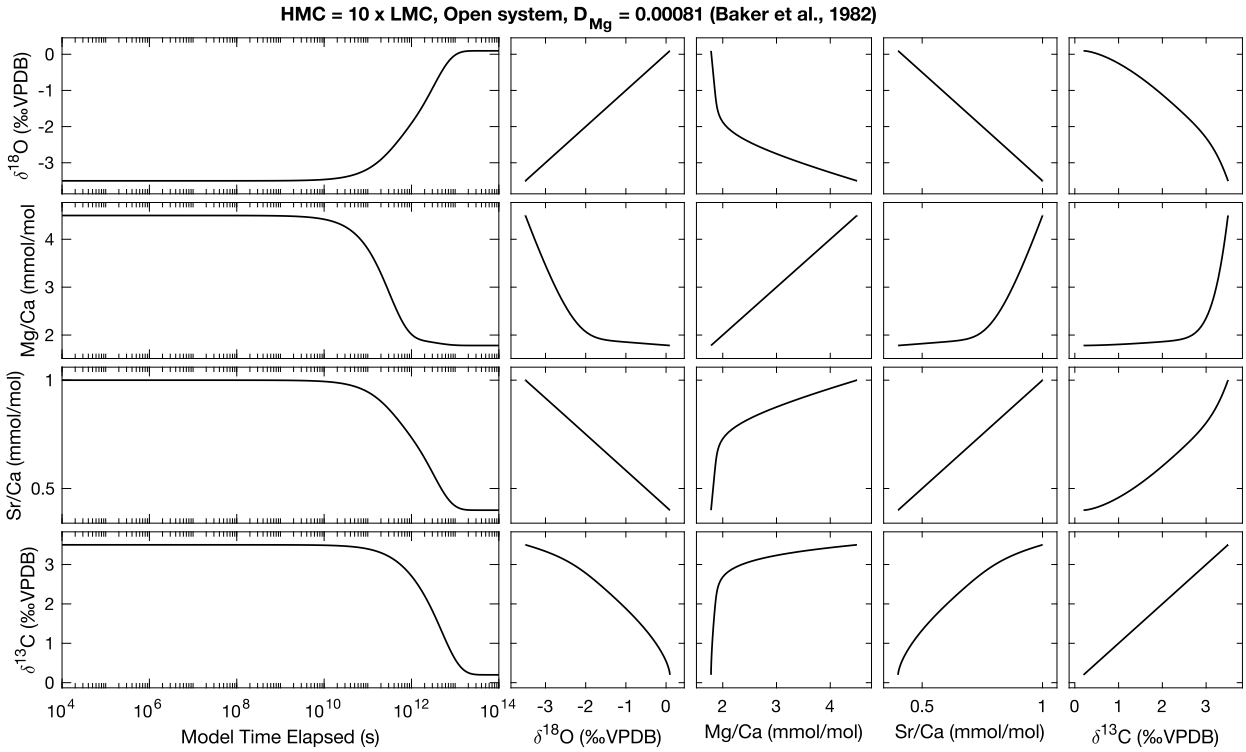

Figure S-21: “open system” model (NDF = 126) output for 0-D model using the Mucci (1987) Mg partitioning coefficient where the HMC component is 10x as reactive as LMC.

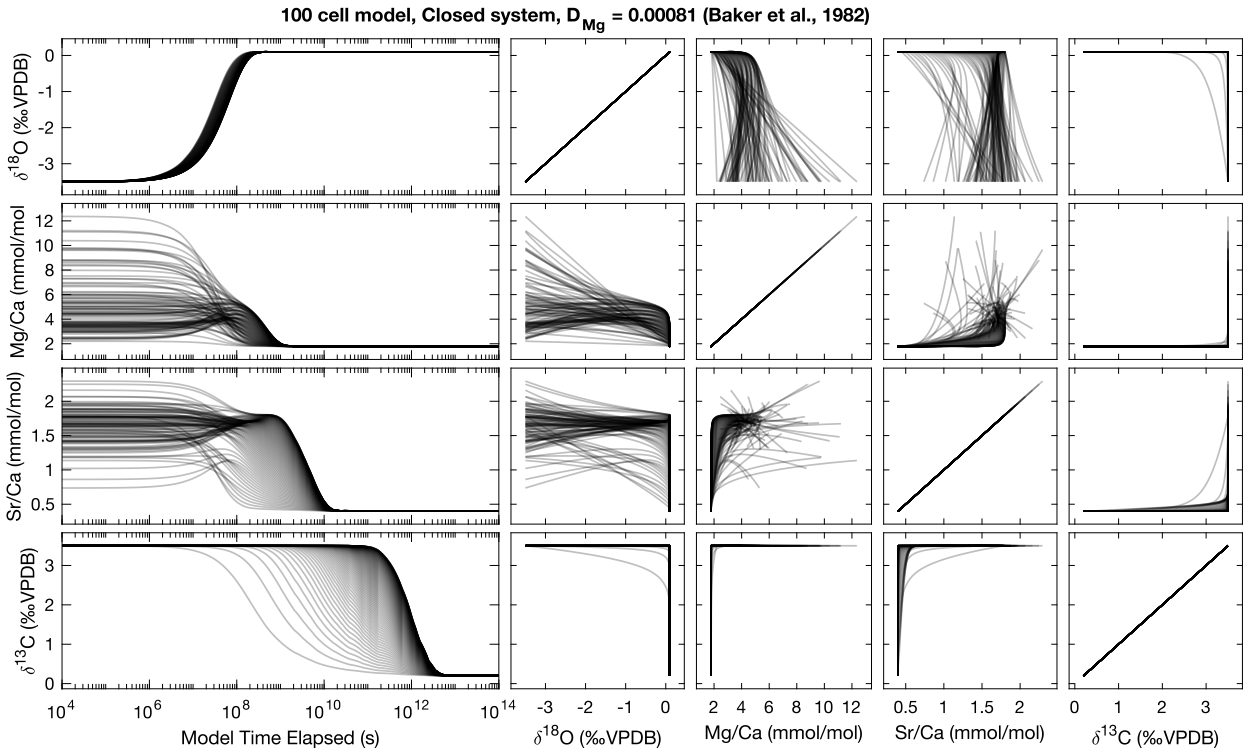

Figure S-22: "closed system" model (NDF = 0.4) output for 1-D model using the Mucci (1987) Mg partitioning coefficient with equal reactivities for HMC and LMC.

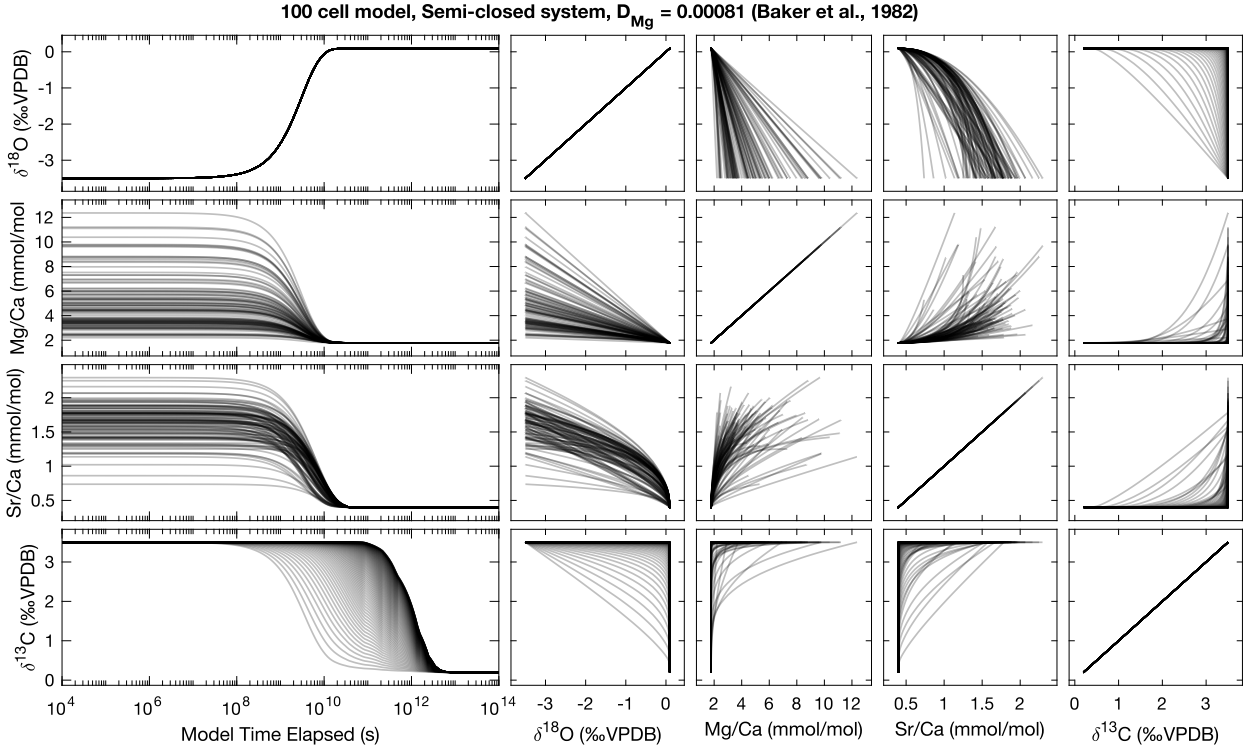

Figure S-23: "semi-closed system" model (NDF = 4) output for 1-D model using the Mucci (1987) Mg partitioning coefficient with equal reactivities for HMC and LMC.

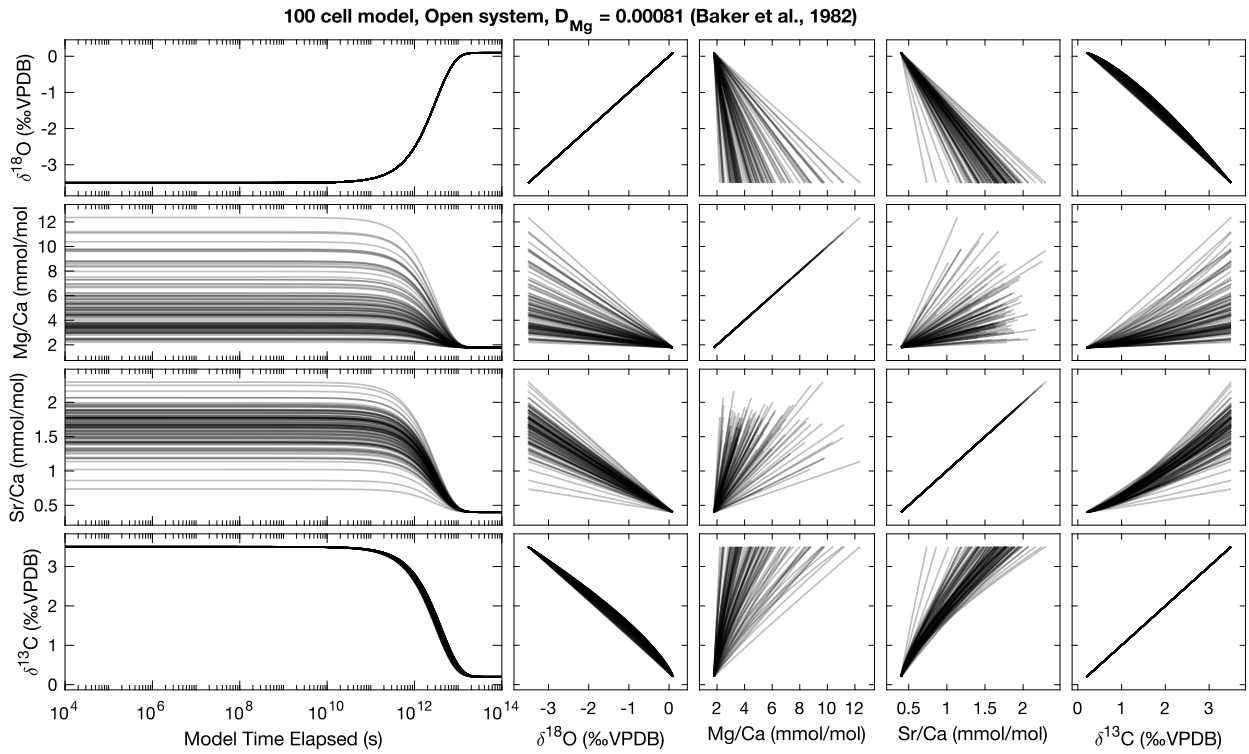

Figure S-24: "open system" model (NDF = 126) output for 1-D model using the Mucci (1987) Mg partitioning coefficient with equal reactivities for HMC and LMC.

Supplementary data files descriptions:

Data S-1: .zip file containing EPMA Mg/Ca and Sr/Ca maps and MATLAB script to generate the components of figure 1 from main text.

Data S-2: .zip file containing MATLAB scripts and associated data for the reaction-diffusion model.

References for supplementary text:

Ahm, A.S.C., Bjerrum, C.J., Blättler, C.L., Swart, P.K., Higgins, J.A., 2018. Quantifying early marine diagenesis in shallow-water carbonate sediments. Geochim. Cosmochim. Acta 236, 140–159. https://doi.org/10.1016/j.gca.2018.02.042

Akanni, K.A., Evans, J.W., Abramson, I.S., 1987. Effective transport coefficients in heterogeneous media. Chem. Eng. Sci. 42, 1945–1954.

Armstrong, J.T., 1988. Quantitative analysis of silicate and oxide materials: comparison of Monte Carlo, ZAF, and phi-rho-z procedures. Microbeam Anal. 239–246.

Baertschi, P., 1976. Absolute 18O content of standard mean ocean water. Earth Planet. Sci. Lett. 31, 341–344. https://doi.org/10.1016/0012-821X(76)90115-1

Baker, P.A., Gieskes, J.M., Elderfield, H., 1982. Diagenesis of Carbonates in Deep-Sea Sediments: Evidence from Sr/Ca Ratios and Interstitial Dissolved Sr2+ Data. J. Sediment. Petrol. 52, 71–82.

Banner, J.L., 1995. Application of the trace element and isotope geochemistry of strontium to

studies of carbonate diagenesis. Sedimentology 42, 805–824. https://doi.org/10.1111/j.1365-3091.1995.tb00410.x
Banner, J.L., Hanson, G.N., 1990. Calculation of simultaneous isotopic and trace element variations during water-rock interaction with applications to carbonate diagenesis. Geochim. Cosmochim. Acta 54, 3123–3137.
Barker, S., Greaves, M., Elderfield, H., 2003. A study of cleaning procedures used for foraminiferal Mg/Ca paleothermometry. Geochemistry, Geophys. Geosystems 4, 1–20. https://doi.org/10.1029/2003GC000559
Beattie, P., Drake, M., Jones, J., Leeman, W., Longhi, J., McKay, G., Nielsen, R., Palme, H., Shaw, D., Takahashi, E., 1993. Terminology for trace-element partitioning. Geochim. Cosmochim. Acta 57, 1605–1606.
Berner, R.A., 1980. Early diagenesis: a theoretical approach. Princeton University Press.
Boudreau, B.P., 1997. Diagenetic models and their implementation. Springer Berlin.
Chang, T., Li, W., 1990. A calibrated measurement of the atomic weight of carbon. Chinese Sci. Bull. 290–296.
Coplen, T.B., Kendall, C., Hopple, J., 1983. Comparison of stable isotope reference samples. Nature 302, 236–238. https://doi.org/10.1038/302236a0
Cramer, B.S., Miller, K.G., Barrett, P.J., Wright, J.D., 2011. Late Cretaceous-Neogene trends in deep ocean temperature and continental ice volume: Reconciling records of benthic foraminiferal geochemistry (δ18O and Mg/Ca) with sea level history. J. Geophys. Res. Ocean. 116, 1–23. https://doi.org/10.1029/2011JC007255
Dekens, P.S., Lea, D.W., Pak, D.K., Spero, H.J., 2002. Core top calibration of Mg/Ca in tropical foraminifera: Refining paleotemperature estimation 3.
Evans, D., Müller, W., 2012. Deep time foraminifera Mg/Ca paleothermometry: Nonlinear correction for secular change in seawater Mg/Ca. Paleoceanography 27, 1–11. https://doi.org/10.1029/2012PA002315
Evans, D., Sagoo, N., Renema, W., Cotton, L.J., Müller, W., Todd, J.A., Saraswati, P.K., Stassen, P., Ziegler, M., Pearson, P.N., Valdes, P.J., Affek, H.P., 2018. Eocene greenhouse climate revealed by coupled clumped isotope-Mg/Ca thermometry. Proc. Natl. Acad. Sci. U. S. A. 115, 1174–1179. https://doi.org/10.1073/pnas.1714744115
Fantle, M.S., Maher, K.M., DePaolo, D.J., 2010. Isotopic approaches for quantifying the rates of marine burial diagenesis. Rev. Geophys. 48.
Henderson, L.M., Kracek, F.C., 1927. The fractional precipitation of barium and radium chromates. J. Am. Chem. Soc. 49, 738–749.
Jurek, K., Renner, O., Krouský, E., 1994. The role of coating densities in X-ray microanalysis. Microchim. Acta 114, 323–326.
Kim, S.T., O'Neil, J.R., 1997. Equilibrium and nonequilibrium oxygen isotope effects in synthetic carbonates. Geochim. Cosmochim. Acta 61, 3461–3475. https://doi.org/10.1016/S0016-7037(97)00169-5
Lear, C.H., Elderfield, H., Wilson, P.A., 2003. A Cenozoic seawater Sr/Ca record from benthic foraminiferal calcite and its application in determining global weathering fluxes. Earth Planet. Sci. Lett. 208, 69–84. https://doi.org/10.1016/S0012-821X(02)01156-1
Lear, C.H., Elderfield, H., Wilson, P.A., 2000. Cenozoic deep-sea temperatures and global ice volumes from Mg/Ca in benthic foraminiferal calcite. Science (80-.). 287, 269–272.

https://doi.org/10.1126/science.287.5451.269
Matthews, M.B., Buse, B., Kearns, S.L., 2019. Electron Probe Microanalysis through Coated Oxidized Surfaces. Microsc. Microanal. 25, 1112–1129. https://doi.org/10.1017/S1431927619014715
Maxwell, J.C., 1881. A treatise on electricity and magnetism. Clarendon press.
Mucci, A., 1987. Influence of temperature on the composition of magnesian calcite overgrowths precipitated from seawater. Geochim. Cosmochim. Acta 51, 1977–1984.
Mulitza, S., Boltovskoy, D., Donner, B., Meggers, H., Paul, A., Wefer, G., 2003. Temperature: δ18O relationships of planktonic foraminifera collected from surface waters. Palaeogeogr. Palaeoclimatol. Palaeoecol. 202, 143–152. https://doi.org/10.1016/S0031-0182(03)00633-3
Petersen, E.E., 1958. Diffusion in a pore of varying cross section. AIChE J. 4, 343–345.
Romanek, C.S., Grossman, E.L., Morse, J.W., 1992. Carbon isotopic fractionation in synthetic aragonite and calcite: effects of temperature and precipitation rate. Geochim. Cosmochim. Acta 56, 419–430.
Simpson, J.H., Carr, H.Y., 1958. Diffusion and nuclear spin relaxation in water. Phys. Rev. 111, 1201.
Smith, M.P., 1986. Silver coating inhibits electron microprobe beam damage of carbonates. J. Sediment. Res. 56, 560–561.
Weissberg, H.L., 1963. Effective diffusion coefficient in porous media. J. Appl. Phys. 34, 2636–2639.